PCCP

The Addition of Methanol to Criegee Intermediates

Journal:	*Physical Chemistry Chemical Physics*
Manuscript ID	CP-ART-06-2019-003480.R1
Article Type:	Paper
Date Submitted by the Author:	23-Jul-2019
Complete List of Authors:	Aroeira, Gustavo; University of Georgia, Chemistry Abbott, Adam; University of Georgia, Computational Chemistry Elliott, Sarah; University of Georgia, Computational Chemistry Turney, Justin; University of Georgia, Center for Computational Chemistry Schaefer, Henry; University of Georgia, Computational Chemistry

PCCP

ARTICLE TYPE

Cite this: DOI: 00.0000/xxxxxxxxxx

The Addition of Methanol to Criegee Intermediates†

Gustavo J. R. Aroeira, Adam S. Abbott, Sarah N. Elliott, Justin M. Turney, and Henry F. Schaefer III*

Received Date
Accepted Date

DOI: 00.0000/xxxxxxxxxx

Bimolecular reactions involving stabilized Criegee intermediates (SCI) have been the target of many studies due to the role these molecules play in atmospheric chemistry. Recently, kinetic rates for the addition reaction of the simplest SCI (formaldehyde oxide) and its methylated analogue (acetone oxide) with methanol were reported both experimentally and theoretically. We re-examine the energy profile of these reactions by employing rigorous *ab initio* methods. Optimized CCSD(T)/ANO1 geometries are reported for the stationary points along the reaction path. Energies are obtained at the CCSD(T)/CBS level of theory. Contributions of full triple and quadruple excitations are computed to assess the convergence of this method. Rate constants are obtained using conventional canonical transition state theory under the rigid rotor harmonic oscillator approximation and with the inclusion of a one-dimensional hindered rotor treatment. These corrections for internal rotations have a significant impact on computed kinetic rate constants. With this approach, we compute rate constants for the addition of methanol to formaldehyde oxide (H_2COO) and acetone oxide [$(CH_3)_2COO$] at 298.15 K as $(1.2\pm0.8)\times10^{-13}$ and $(2.8\pm1.3)\times10^{-15}$ cm^3 s^{-1}, respectively. Additionally, we investigate the temperature dependence of the rate constant, concluding that the transition state barrier height and tunneling contributions shape the qualitative behaviour of these reactions.

1 Introduction

Carbonyl oxides, commonly known as Criegee intermediates (CI), first gained attention as intermediates in the ozonolysis of alkenes.[1] The detailed study of these molecules was made viable by the development of strategies to produce them in laboratory.[2,3] Now, the major source of atmospheric CIs is thought to be the oxidation of alkenes by ozone,[4] and the role of these molecules, as well as their stabilities, have been the target of debate in recent years.

Many of the Criegee intermediates produced through ozonolysis have high internal energy ("hot CI") and will rapidly undergo unimolecular reactions. However, a significant fraction (around 42% for the simplest CI, H_2COO) is predicted to be collisionally stabilized,[5] and thus can participate in bimolecular reactions. It was also observed that, for some alkenes precursors, there is a nascent fraction of CIs formed with insufficient internal energy to surpass unimolecular reactions barriers.[6] Therefore, stabilized Criegee intermediates (SCI) could be formed when ozone reacts with alkenes in the atmosphere.[7] These SCIs are expected to react with others gases, such as sulfur dioxide (SO_2) to produce sulfuric acid (H_2SO_4), which can contribute to aerosol formation.[8] The important role SCIs may play in tropospheric chemistry has motivated several studies to examine its reactions with species such as H_2O,[9–13] SO_2,[3,14–17] NO_2,[3,14] NH_3,[18,19] carboxylic acids,[20,21] aldehydes[22,23] and alcohols.[24–26] These studies show that the reaction rate depends strongly on the structure of the SCI.[27] For example, the *anti* conformer of acetaldehyde oxide (CH_3CHOO) is more reactive towards water than its *syn* conformer.[14] Moreover, acetone oxide [$(CH_3)_2COO$], unlike the simplest CI, is relatively unreactive towards water, but rapidly reacts with SO_2.[28,29] Unimolecular decomposition can account for more than half of SCI loss in the atmosphere.[30] Despite the relatively slow reaction rate, the reaction with water is thought to be the major sink of the remaining SCIs,[31] as water is ubiquitous in the atmosphere.

The reaction of CIs and alcohols is known to produce α-alkoxyalkyl hydroperoxides and peracids. Neeb and coworkers noticed that methoxymethyl hydroperoxide (MMHP) is obtained when ozonolysis of ethene takes place in the presence of methanol.[32] They attributed this product to the reaction of methanol with the simplest CI, formaldehyde oxide. This chemistry is also likely to take place in nature, because alcohols are commonly found in the atmosphere and methanol is the most

Center for Computational Quantum Chemistry, University of Georgia, 140 Cedar Street, Athens, Georgia 30602, USA. E-mail: ccq@uga.edu; Fax: +1 706 542-0406; Tel: +1 706 542-2067

† Electronic Supplementary Information (ESI) available: Optimized geometries, harmonic frequencies, heat of formation, and hindered rotor scans. See DOI: 10.1039/cXCP00000x/

abundant organic component after methane.[33] Moreover, since both alcohols and alkenes are released from biogenic sources, such as plant emissions,[34] one may expect considerable co-location of alcohols and SCIs.[24]

The reaction of SCIs with organic compounds, such as alcohols, will often generate low-volatility products that can contribute to secondary aerosol formation.[35,36] The atmosphere offers an extensive range of possibilities for bimolecular reactions involving SCIs. Consequently, several kinetic studies have been performed to determine which reactions are significant sinks for Criegee intermediates. Tobias and Ziemman measured the relative rate of reactions of several molecules with a long-chain SCI and the observed rates increased in the order: water $\ll$ methanol $<$ 2-propanol $\ll$ formaldehyde $<$ formic acid $<$ heptanoic acid.[37] McGillen and coworkers used cavity ring down spectroscopy to measure kinetics for reactions of SCI and alcohols over a range of temperature and pressures.[24] They found a negative temperature dependence for the rate of addition of methanol to formaldehyde oxide (H_2COO). On the other hand, the rate of addition of methanol to acetone oxide [$(CH_3)_2COO$] presented both positive and negative temperature dependence, where the reaction rate decreases until an inflection point (around 300 K), after which it increases with temperature. In that same study, ethanol addition to SCIs was also examined, but they concluded that the chain length on the alcohol does not affect the reaction rate significantly.[24] In a more recent work, Tadayon, Foreman and Murray used a flash photolysis flow reactor to measure the rate for the addition of alcohols to SCI.[25] They found rate constants of $(1.4 \pm 0.4) \times 10^{-13}$ cm^3 s^{-1} and $(2.3 \pm 0.6) \times 10^{-13}$ cm^3 s^{-1} for the reaction of formaldehyde oxide at 295 K with methanol and ethanol respectively,[25] in good agreement with the work by McGillen and coworkers.[24]

Both experimental studies described above also provided supporting *ab initio* computations. Tadayon and coworkers reported energies for the formaldehyde oxide reaction with methanol at the CCSD(T)/aug-cc-pVTZ level of theory using CCSD/cc-pVDZ geometries. McGillen and coworkers computed relative energies for the addition of methanol to both formaldehyde oxide and acetone oxide at DF-LCCSD(T)-F12a/aug-cc-pVTZ level of theory on B3LYP/aug-cc-pVTZ geometries.[24] For both reactions, the pre-reactive complex and transition state barrier were each observed to lie energetically below the reactants. Zero-point vibrational energy corrections, however, were not included in the relative energies of the reaction surface. The authors acknowledge that a more rigorous treatment for this system is needed.

Indeed, past literature results indicate that reactions involving SCIs are particularly sensitive to the treatment of electron correlation. Although CCSD(T) is capable of reproducing the experimental geometry of the simplest SCI,[38] some studies indicate that the excitations beyond perturbative triples contribute significantly to the energy of transition states involving SCIs. For example, in the 1,4-hydrogen transfer reaction of the propionaldehyde oxide (CH_3CH_2CHOO), the inclusion of full triples and perturbative quadruples elevated the transition state by 0.43 kcal mol^{-1}.[39] Moreover, this correlation treatment further raises barriers by 0.70 kcal mol^{-1} when formaldehyde oxide (H_2COO) reacts with water[40] and 0.84 kcal mol^{-1} when it reacts with ammonia.[18] This suggests that, due to the complicated electronic structure of SCIs, corrections for electron correlation beyond CCSD(T) may be necessary to achieve quantitative results.

In this work, we use high-level theoretical methods to study the potential energy surface of the reaction of formaldehyde oxide (H_2COO) and acetone oxide [$(CH_3)_2COO$] with methanol:

$$CH_3OH + H_2COO \longrightarrow CH_3OCH_2OOH \quad \text{(R1)}$$

$$CH_3OH + (CH_3)_2COO \longrightarrow CH_3OC(CH_3)_2OOH \quad \text{(R2)}$$

These results are used to discuss differences observed in the kinetics based on the structure of the Criegee intermediate involved.

2 Computational Methods

Geometries for each species investigated were optimized via analytic gradients using coupled cluster theory with single, double, and perturbative triple excitations [CCSD(T)] and the roughly triple-ζ quality variant of the atomic natural orbital basis set (ANO),[41,42] commonly denoted as ANO1. The convergence of single-point energies with respect to basis set and level of theory was observed by employing the Focal Point Approach (FPA) of Allen and coworkers.[43–45] For each species Hartree–Fock energies were calculated using the Dunning correlation consistent basis sets,[46] cc-pVXZ (X = D, T, Q, 5). Correlation energies were obtained using second-order Møller–Plesset perturbation theory (MP2), CCSD, and CCSD(T) with the cc-pVXZ (X = D, T, Q) basis sets. The subsequent complete basis set limit (CBS) extrapolation used a three-point formula for SCF energies[47,48] and two-point formula for correlation energies.[49] All computations of energy and geometry optimizations were perfomed using the frozen core approximation. Energies are presented at the CCSD(T)/CBS+Δ level of theory, where Δ stands the for additive corrections:

$$\Delta = \Delta_{\mathrm{ZPVE}} + \Delta_{\mathrm{CORE}} + \Delta_{\mathrm{DBOC}} + \Delta_{\mathrm{REL}}$$

Zero-point vibrational energy corrections (Δ_{ZPVE}) in the harmonic approximation were obtained using CCSD(T) level of theory with ANO1 basis set for reaction R1 and with the ANO0 basis set for reaction R2. The correction for the frozen core approximation (Δ_{CORE}) was estimated as the difference between the all-electron (AE) and frozen-core (FC) energies using a weighted core-valence cc-pwCVTZ basis set:[50]

$$\Delta_{\mathrm{CORE}} = E_{\text{AE-CCSD(T)}} - E_{\text{FC-CCSD(T)}}$$

The diagonal Born–Oppenheimer correction (Δ_{DBOC}) was obtained at the CCSD level using the ANO0 basis set.[51,52] Corrections for scalar relativistic effects (Δ_{REL}) were computed using the spin-free X2C-1e method with an X2C-recontracted correlation-consistent cc-pCVTZ basis set.[53–58] The relativistic correction was taken as:

$$\Delta_{\mathrm{REL}} = E_{\text{AE-CCSD(T)/X2C-1e}} - E_{\text{AE-CCSD(T)}}$$

Finally, contributions of full triple and perturbative quadruple excitations ($\Delta_{\mathrm{T(Q)}}$) were computed to test the reliability of the

CCSD(T) method for these reactions and to estimate the error associated with electron correlation. Energies including this correction are denoted as CCSD(T)/CBS+Δ+$\Delta_{T(Q)}$. This computation was performed using the cc-pVDZ and 6-31G* basis sets, for reactions R1 and R2 respectively, as follows:

$$\Delta_{T(Q)} = E_{CCSDT(Q)} - E_{CCSD(T)}$$

The MOLPRO 2010.1 package[59] was used to compute CCSD(T)/cc-pVXZ single point energies used in the FPA. Geometry optimization and additive corrections, including CCSDT(Q) computations were performed using the CFOUR 2.0 quantum chemistry package.[60] Torsional scans, utilized in the construction of partition functions, were computed using the density fitted second-order Møller–Plesset perturbation theory (DF-MP2) with the cc-pVTZ basis set available in the Psi4 package.[61] The rotational scans are available in our supporting information (Figures S1–S31); only torsions with barriers lower than 15 kcal mol^{-1} were treated with the one-dimensional hindered rotor approach. These modes were projected from the CCSD(T) Hessian (ANO1 or ANO0 for reaction R1 and R2, respectively). With the resulting frequencies, CCSD(T)/ANO1 geometry, and energy profiles for the hindered rotors as input parameters, the Master Equation System Solver (MESS) code enabled us to solve for one-dimensional hindered rotor partition function.[62,63]

3 Results and Discussion

3.1 Geometries

Selected geometric parameters obtained for the two Criegee intermediates studied in this work are presented in Figure 1. The formaldehyde oxide (H_2COO) CCSD(T)/ANO1 optimized structure agrees very well with the experimental geometry determined by Nakajima and coworkers.[38] The CCSD(T)/ANO1 bond length for C−O is just 0.005 Å longer than the experimental value, while the B3LYP/aug-cc-pVTZ structure underestimates the C−O bond length by about 0.02 Å . These geometric parameters are particularly important for Criegee intermediates because the relative C−O and O−O bonds distances are indicative of the electronic structure of the C−O−O moiety. Historically, Criegee intermediates have been described using two different representations: as a biradical or a zwitterion.[64] Accurate *ab initio* methods predict π character in the C−O bond, thus supporting the zwitterionic picture.[65,66] Su and coworkers have suggested that the infrared absorption spectrum of the simplest CI (H_2COO) also supports a double bond (C=O) model and used this feature to explain the rapid self-reaction predicted for this molecule.[67,68] Here, we observe that acetone oxide [$(CH_3)_2COO$] has a slightly shorter C−O bond (∼0.002 Å) and a longer O−O bond (∼0.033 Å) when compared to its non-methylated counterpart, suggesting that the methyl groups can enhance the zwitterionic character. This effect, however, is not clear using the B3LYP method, where both C−O and O−O bonds are stretched.

Optimized structures for stationary points along the reaction of methanol with formaldehyde oxide (H_2COO) and acetone oxide [$(CH_3)_2COO$] are shown in Figures 2 and 3, respectively. Both systems contain a hydrogen bonded pre-reactive complex, where

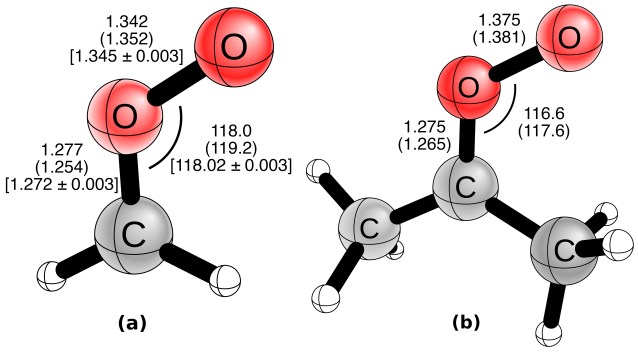

Fig. 1 Selected geometric parameters of CCSD(T)/ANO1 optimized SCIs: (a) formaldehyde oxide (b) acetone oxide. Bond lengths are given in Ångstrom. Values in parentheses are previously reported B3LYP/aug-cc-pVTZ[24] parameters and in brackets are experimental values.[38]

the C−O bond of the SCI is further shortened, whereas the O−O bond is stretched. This indicates an increased zwitterionic character of SCI once the complex is formed. The pre-reactive complex shows sensitivity to steric hindrance when methyl substituents are added; the intermolecular distance between the oxygen of the methanol and the central carbon of the SCI is greater for the acetone oxide complex by 0.264 Å when compared to the simplest SCI. In the transition state, for both reactions, the intermolecular carbon-oxygen distance is shortened by at least 0.8 Å as a bond is being formed between these two atoms. Similarly, the hydrogen bond that holds the complex together becomes shorter by about 0.2 Å as the proton transfer completes. Finally, the product hydroperoxide presents C−O and O−O bond distances that are typical of single bonds. Thus, based on geometric parameters, we expect the products of each reaction to have no resonance structures. The most significant differences between the geometries reported here and the B3LYP/aug-cc-pVTZ structures available in the literature[24] are observed in the products. For these, the internal hydrogen bonds are determined to be at least 0.22 Å shorter at the CCSD(T)/ANO1 level of theory, which we expect will lead to more accurate energies. The pre-reactive complex reported by McGillen and coworkers[24] had the formaldehyde oxide (H_2COO) in the same plane as the C−O bond of the methanol, whereas our structure is slightly bent. Both configurations are minima in the potential energy surface and are virtually degenerate, but our intrinsic reaction coordinate (IRC) calculations indicate that the bent structure is the true pre-reactive complex.

In a recent study, Watson and coworkers[69] reported additional transition states, including a path where methanol acts as a catalyst to a 1,4-H transfer in the acetone oxide molecule. These pathways have, however, higher barrier heights, therefore, would not shift kinetics rates significantly.

3.2 Energies

Tables 1 and 2 show the incremented focal point table for the formaldehyde oxide (H_2COO) and acetone oxide [$(CH_3)_2COO$] systems, respectively. In all cases there is a good convergence with respect to basis set. However, we predict large corrections by including full triple and perturbative quadruple excitations.

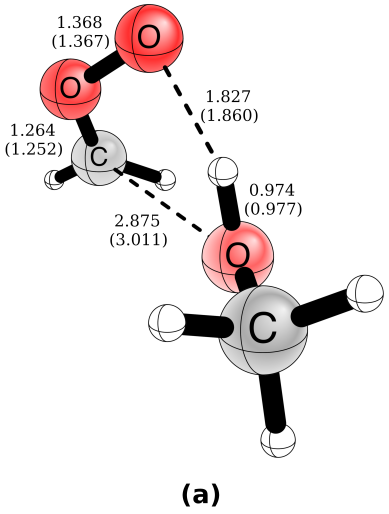

Fig. 2 Optimized CCSD(T)/ANO1 geometries for the addition of methanol to formaldehyde oxide: (a) pre-reactive complex (b) transition state (c) product. Bond lengths are given in Ångstrom. Values in parentheses are previously reported B3LYP/aug-cc-pVTZ parameters from Ref. 24.

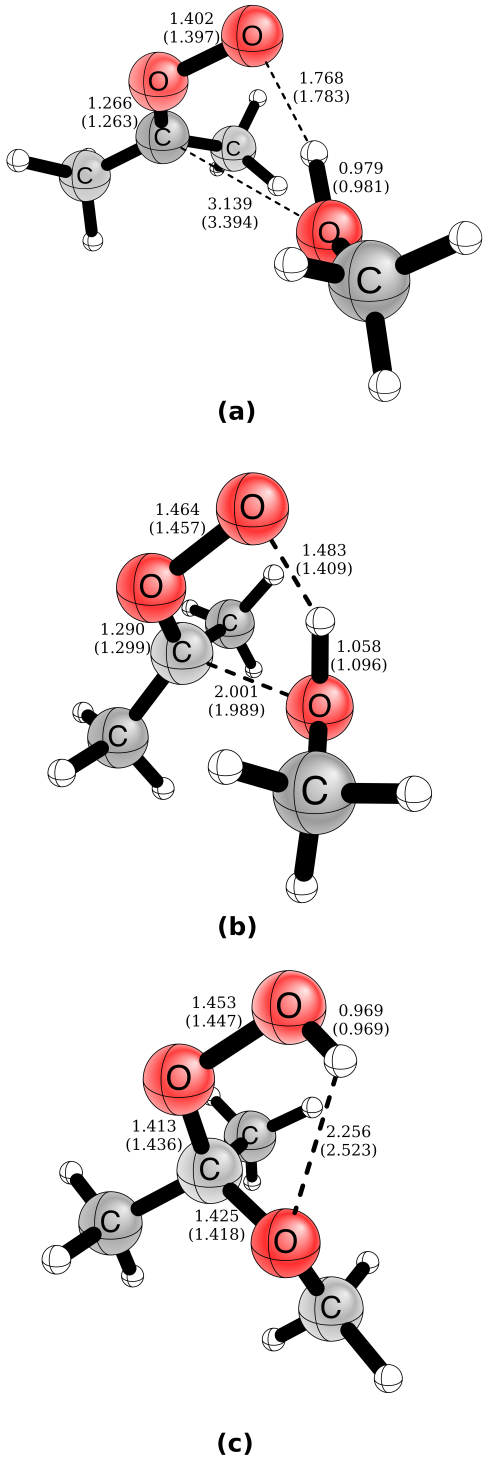

Fig. 3 Optimized CCSD(T)/ANO1 geometries for the addition of methanol to acetone oxide: (a) pre-reactive complex (b) transition state (c) product. Bond lengths are given in Ångstrom. Values in parentheses are previously reported B3LYP/aug-cc-pVTZ parameters from Ref. 24.

This result is aligned with other studies on systems with Criegee intermediates[18,39,40] and it is normally understood as a consequence of the multireference character of SCIs; t_1 diagnostics[70] for formaldehyde oxide and acetone oxide are 0.045 and 0.033, respectively. These corrections of 0.83 and 0.60 kcal mol^{-1} for reactions R1 and R2, respectively, result in a dramatic change in their transition state barriers: for acetone oxide the barrier height is raised nearly 4-fold when this contribution is included. To assess whether these high-order correlation corrections are reliable, we computed the heat of formation at 0 K ($\Delta H_f^{0\,\mathrm{K}}$) for the formaldehyde oxide at the CCSD(T)/CBS, CCSDT(Q)/CBS, and CCSDTQ/CBS level of theory (see supporting information). For these $\Delta H_f^{0\,\mathrm{K}}$ values we obtain 27.12, 25.72 and 26.35 kcal mol^{-1}, respectively; while the reference value available in the Active Thermochemical Tables (ATcT) is 26.74 ± 0.15 kcal mol^{-1}.[71–73] The CCSD(T) and CCSDTQ values differ from the reference by less than 0.4 kcal mol^{-1}; however, the CCSDT(Q) result differs by nearly 1.0 kcal mol^{-1}. This indicates that contributions evaluated at the CCSDT(Q) level of theory should be taken with caution, as the perturbative treatment for quadruple excitations might be producing spurious results.

Additive corrections for the Born–Oppenheimer approximation, frozen core, and scalar relativistic effects are smaller than 0.17 kcal mol^{-1} in all cases, thus validating the employment of such approximations herein. Although a satisfactory convergence of relative energy with respect to method and basis set is observed, the large contribution of higher-order excitations implies in a large uncertainty. Based on the results for the heat of formation, we believe that the correct barrier for the transition state in each reaction should lie between the CCSD(T)/CBS+Δ and CCSD(T)/CBS+Δ+$\Delta_{\mathrm{T(Q)}}$ values, and hence we estimate our uncertainty from this interval. Our final energies are expressed as shown in equation 1, where E_{min} is the energy predicted by the CCSD(T)/CBS+Δ level of theory and E_{max} is the value computed by the CCSD(T)/CBS+Δ+$\Delta_{\mathrm{T(Q)}}$ level of theory.

$$E_{\mathrm{final}} = \left(\frac{E_{\mathrm{min}} + E_{\mathrm{max}}}{2}\right) \pm \frac{\Delta_{\mathrm{T(Q)}}}{2} \qquad (1)$$

Figure 4 depicts the potential energy surface along the reaction coordinate for both systems studied in this work. The energy profiles obtained agree qualitatively with previous results available in the literature.[24,25,69] The addition of methanol to formaldehyde oxide proceeds through the formation of a pre-reactive complex that lies 7.24 ± 0.18 kcal mol^{-1} below the reagents. The transition state between the complex and the product is submerged by 1.48 ± 0.42 kcal mol^{-1} and the product, methoxymethyl hydroperoxide, lies 46.53 ± 0.78 kcal mol^{-1} below the reactants. The reaction of methanol with acetone oxide also forms a pre-reactive complex lying below the reagents by 8.94 ± 0.18 kcal mol^{-1}. The transition state, however, is predicted to lie 0.54 ± 0.30 kcal mol^{-1} above the reagents. The methoxyisopropyl hydroperoxide product is formed with an excess of energy of 35.04 ± 0.59 kcal mol^{-1}. The energies of the transition states are the key difference observed between the two reactions under study. The inclusion of methyl groups on the SCI raises the barrier of the reaction above the reagents and changes the qualitative behavior of the computed kinetic rate constant over a range of temperatures. This impact will be further discussed in the next session. The agreement of our energies with the recent work by Watson and coworkers[69] (H_2COO) system is fairly good. Their computed DF-LCCSD(T)-F12a/aug-cc-pVTZ transition state barrier heights are within our range of uncertainty. However, this apparent agreement seems to be accidental, since for the smaller SCI (H_2COO) their value is closer to our CCSD(T)/CBS+Δ result, whereas for the bigger SCI [$(CH_3)_2COO$] their energy approaches our CCSD(T)/CBS+Δ+$\Delta_{\mathrm{T(Q)}}$ value.

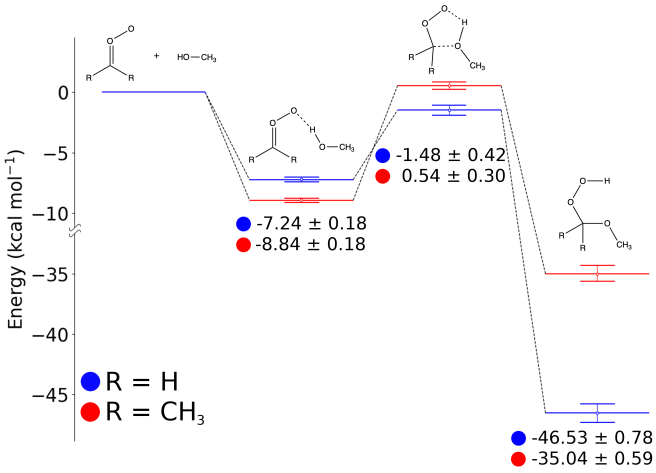

Fig. 4 Potential energy surface along the reaction path of the addition of methanol to a Criegee intermediate. Uncertainties are taken as the interval between the CCSD(T)/CBS+Δ and CCSD(T)/CBS+Δ+$\Delta_{\mathrm{T(Q)}}$ methods, whereas central values are the average of them, as shown in equation 1.

3.3 Kinetics

3.3.1 Model.

Following the reaction mechanism established in the literature[24,25,69] and supported by this present work, chemical equation 2 gives a reasonable description of the process. Due to the high exothermicity, the second step of the reaction is considered irreversible.

$$\mathrm{SCI} + \mathrm{A} \underset{k_{-1}}{\overset{k_1}{\rightleftharpoons}} \mathrm{SCI{\cdots}A} \xrightarrow{k_2} \mathrm{P} \qquad (2)$$

The rate of formation of the product (P) depends on the concentration of the pre-reactive complex (SCI···A) as shown in equation 3. This problem can be simplified using the steady-state approximation (SSA),[74] which yields equation 4. Additionally, a final approximation is often suitable for this class of reactions: if we assume that $k_2 \ll k_{-1}$ the expression can be reduced to equation 5. Here the total reaction rate (k_{tot}) is a product of the forward reaction rate (k_2) and the equilibrium constant of the pre-reactive

Table 1 Incremented focal point table for reaction R1 involving formaldehyde oxide (H_2COO). Energies are given in kcal mol^{-1} relative to the reactants. Final values are computed at the CCSD(T)/CBS+Δ level of theory, where $\Delta = \Delta_{\mathrm{ZPVE}}^{\mathrm{ANO1}} + \Delta_{\mathrm{CORE}} + \Delta_{\mathrm{DBOC}} + \Delta_{\mathrm{REL}}$, with and without the correction for higher order excitation ($\Delta_{\mathrm{T(Q)}}$) computed with the cc-pVDZ basis set

Basis set	ΔE_e RHF	δ MP2	δ CCSD	δ CCSD(T)	ΔE_e NET
			Pre–reactive complex		
cc-pVDZ	–13.37	+1.97	+0.21	+1.05	–10.13
cc-pVTZ	–11.32	+0.70	+0.08	+0.80	–9.74
cc-pVQZ	–10.59	+0.58	–0.12	+0.72	–9.42
cc-pV5Z	–10.20	[+0.53]	[–0.20]	[+0.69]	[–9.17]
CBS	[–9.95]	[+0.49]	[–0.27]	[+0.65]	[**–9.08**]
CCSD(T)/CBS+Δ:	–9.08 + 1.67 + 0.00 – 0.02 + 0.01		= **–7.42**		
CCSD(T)/CBS+Δ+$\Delta_{\mathrm{T(Q)}}$:	–9.08 + 1.67 + 0.00 – 0.02 + 0.01 + 0.35 = **–7.07**				
			Transition state		
cc-pVDZ	–7.07	–2.19	+2.97	+0.75	–5.54
cc-pVTZ	–3.21	–4.79	+2.70	+0.23	–5.08
cc-pVQZ	–1.97	–5.07	+2.30	+0.05	–4.69
cc-pV5Z	–1.42	[–5.17]	[+2.16]	[–0.01]	[–4.44]
CBS	[–1.11]	[–5.28]	[+2.01]	[–0.07]	[**–4.45**]
CCSD(T)/CBS+Δ:	–4.45 + 2.45 + 0.14 – 0.03 – 0.01		= **–1.90**		
CCSD(T)/CBS+Δ+$\Delta_{\mathrm{T(Q)}}$:	–4.45 + 2.45 + 0.14 – 0.03 – 0.01 + 0.83 = **–1.07**				
			Product		
cc-pVDZ	–61.13	+0.35	+3.83	+3.86	–53.09
cc-pVTZ	–58.22	–1.21	+2.88	+3.60	–52.95
cc-pVQZ	–56.75	–1.13	+2.22	+3.54	–52.12
cc-pV5Z	–56.16	[–1.11]	[+1.98]	[+3.52]	[–51.76]
CBS	[–55.84]	[–1.08]	[+1.73]	[+3.50]	[**–51.69**]
CCSD(T)/CBS+Δ:	–51.69 + 4.31 + 0.01 – 0.02 + 0.09		= **–47.31**		
CCSD(T)/CBS+Δ+$\Delta_{\mathrm{T(Q)}}$:	–51.69 + 4.31 + 0.01 – 0.02 + 0.09 + 1.56 = **–45.75**				

Table 2 Incremented focal point table for reaction R2 involving acetone oxide [$(CH_3)_2COO$]. Energies are given in kcal mol^{-1} relative to the reactants. Final values are computed at the CCSD(T)/CBS+Δ level of theory, where $\Delta = \Delta_{\mathrm{ZPVE}}^{\mathrm{ANO0}} + \Delta_{\mathrm{CORE}} + \Delta_{\mathrm{DBOC}} + \Delta_{\mathrm{REL}}$, with and without the correction for higher order excitation ($\Delta_{\mathrm{T(Q)}}$) computed with the 6-31G* basis set

Basis set	ΔE_e RHF	δ MP2	δ CCSD	δ CCSD(T)	δE_e NET
			Pre–reactive complex		
cc-pVDZ	–13.27	–1.58	+1.24	+0.42	–13.18
cc-pVTZ	–10.60	–2.67	+1.03	+0.12	–12.13
cc-pVQZ	–9.67	–2.59	+0.80	+0.05	–11.42
cc-pV5Z	–9.22	[–2.56]	[+0.71]	[+0.02]	[–11.04]
CBS	[–8.96]	[–2.53]	[+0.63]	[–0.00]	[**–10.86**]
CCSD(T)/CBS+Δ:	–10.86 + 1.77 – 0.01 – 0.03 + 0.01		= **–9.12**		
CCSD(T)/CBS+Δ+$\Delta_{\mathrm{T(Q)}}$:	–10.86 + 1.77 – 0.01 – 0.03 + 0.01 + 0.35 = **–8.77**				
			Transition state		
cc-pVDZ	+3.62	–12.16	+4.44	–1.03	–5.13
cc-pVTZ	+8.25	–14.25	+4.47	–1.64	–3.17
cc-pVQZ	+9.71	–14.09	+4.19	–1.77	–1.96
cc-pV5Z	+10.31	[–14.04]	[+4.09]	[–1.81]	[–1.45]
CBS	[+10.62]	[–13.98]	[+3.99]	[–1.86]	[**–1.23**]
CCSD(T)/CBS+Δ:	–1.23 + 1.35 + 0.17 – 0.04 + 0.00		= **+ 0.24**		
CCSD(T)/CBS+Δ+$\Delta_{\mathrm{T(Q)}}$:	–1.23 + 1.35 + 0.17 – 0.04 + 0.00 + 0.60 = **+ 0.84**				
			Product		
cc-pVDZ	–40.28	–9.50	+4.66	+1.93	–43.19
cc-pVTZ	–37.04	–10.33	+4.06	+1.58	–41.73
cc-pVQZ	–35.53	–9.86	+3.60	+1.57	–40.23
cc-pV5Z	–34.92	[–9.69]	[+3.43]	[+1.56]	[–39.62]
CBS	[–34.59]	[–9.52]	[+3.26]	[+1.56]	[**–39.29**]
CCSD(T)/CBS+Δ:	–39.29 + 3.53 + 0.06 – 0.02 + 0.09		= **–35.62**		
CCSD(T)/CBS+Δ+$\Delta_{\mathrm{T(Q)}}$:	–39.29 + 3.53 + 0.06 – 0.02 + 0.09 + 1.17 = **–34.45**				

complex formation (K_c)

$$\frac{d[P]}{dt} = k_2[\mathrm{SCI}\cdots\mathrm{A}] \tag{3}$$

$$\xrightarrow{SSA} k_2 \frac{k_1}{k_{-1}+k_2}[\mathrm{SCI}][\mathrm{A}] \tag{4}$$

$$\xrightarrow{k_2 \ll k_{-1}} k_2 \frac{k_1}{k_{-1}}[\mathrm{SCI}][\mathrm{A}] = k_2 K_c[\mathrm{SCI}][\mathrm{A}] \tag{5}$$

The equilibrium constant can be obtained using the partition function of each species, whereas the rate constant, k_2, can be obtained using conventional canonical transition state theory (CTST).[75,76] Expressed in terms of per volume partition functions, these are

$$K_c = \frac{q_{\mathrm{SCI}\cdots\mathrm{A}}}{q_{\mathrm{SCI}} q_{\mathrm{A}}} \tag{6}$$

$$k_2 = \kappa \frac{k_B T}{h} \frac{q_{\mathrm{TS}}}{q_{\mathrm{SCI}\cdots\mathrm{A}}} \tag{7}$$

where κ is the transmission coefficient, k_B is the Boltzmann constant, h is Planck's constant, and T is the temperature. If we set the energy of the reactants equal to zero, the electronic partition function can be simplified and factored out to give the final expression:

$$k_{\mathrm{tot}} = k_2 K_c = \kappa \frac{k_B T}{h} \frac{q^{\mathrm{trv}}_{\mathrm{TS}}}{q^{\mathrm{trv}}_{\mathrm{SCI}} q^{\mathrm{trv}}_{\mathrm{A}}} e^{-\frac{E_{\mathrm{TS}}}{k_B T}} \tag{8}$$

where q^{trv} is the per volume partition function that includes translational, rotational, and vibrational degrees of freedom, and E_{TS} is the energy of the transition state relative to reactants, including ZPVE. Therefore, aside from the transmission coefficient, within this model the overall rate constant depends on the nature of the transition state and reagents, but not on the pre-reactive complex. Alternatively, one can write the thermodynamic formulation of this model, as shown in equation 9, where p stands for the pressure for which the Gibbs free energy was computed. This formulation is completely equivalent to equation 8. This model was used before to study the addition of ammonia to SCIs,[18] yielding satisfactory results that were subsequently validated experimentally.[77] The approach also has become the conventional method to compute theoretical rate constants for the reaction of alcohols and SCIs.[25,69]

$$k_{\mathrm{tot}} = \kappa \frac{k_B T}{h} \frac{k_B T}{p} e^{-\frac{\Delta G_{\mathrm{TS}}}{k_B T}} \tag{9}$$

3.3.2 Rate constants at 298.15 K.

Tadayon and coworkers[25] computed the rate of the reaction of methanol and formaldehyde oxide (H_2COO) using CCSD(T)/aug-cc-pVTZ//CCSD/cc-pVDZ energies, paired with the kinetic model underlying equation 9. They obtained results in good agreement with experimental data, approximately greater by a factor of 2. However, in a recent computational work, Watson and coworkers[69] supplied this same kinetic model with DF-CCSD(T)-F12/aug-cc-pVTZ//B3LYP/aug-cc-pVTZ energies and, despite using arguably more reliable electronic structure methods, obtained rate constants one order of magnitude less than the experimental values. This disparity suggests potential error cancellation between the limitations of the kinetic approach and the imprecision in the energies reported by Tadayon and coworkers.[25] This could explain why their treatment was not able to reproduce experimental trends when different alcohols reacted with SCIs. Watson and coworkers[69] argued that the differences between their computed rate constants and the experimental values obtained by McGillen and coworkers[24] were due to variations in pressure: experimental values were obtained at 10 Torr while theoretical values were computed at standard pressure. However, equation 8 demonstrates that there is no pressure dependence in the model, since the per volume partition functions depend only on temperature. CTST, in fact, assumes the high pressure limit. We suspect that Watson and coworkers introduced pressure dependence in the pre-exponential factor of equation 9, but they likely neglected the pressure dependence of ΔG in the exponential factor, which would cancel out the former. Moreover, the experimental data reported by McGillen and coworkers[24] contain some measurements at 100 Torr and no significant differences are observed with respect to the values obtained at lower pressure. This supports the use of the pressure independent CTST for this system over other kinetic models.

Table 3 presents our kinetic rate constants at 298.15 K for both reactions under investigation; similarly to our energies, we obtained rate constants by averaging a maximum value (k_{max}) computed with the CCSD(T)/CBS+Δ method with a minimum value (k_{min}) obtained with the CCSD(T)/CBS+Δ+$\Delta_{\mathrm{T(Q)}}$ method, as shown in equation 10.

$$k_{\mathrm{final}} = \left(\frac{k_{\mathrm{min}} + k_{\mathrm{max}}}{2}\right) \pm \frac{\Delta k}{2} \tag{10}$$

The tunneling factor (κ) was obtained from an asymmetric Eckart function.[78,79] Partition functions computed under the rigid-rotor harmonic oscillator (RRHO) approximation provided rate constants of $(3.0\pm1.8)\times10^{-14}$ cm^3 s^{-1} for formaldehyde oxide (H_2COO). For acetone oxide [$(CH_3)_2COO$] a rate constant of $(2.8\pm1.3)\times10^{-16}$ cm^3 s^{-1} was obtained. When partition functions are improved by utilizing a one-dimensional hindered rotor (1-D HR) treatment for low-frequency modes corresponding to internal rotations (see supporting information), the rate constant for the first reaction is increased by a factor of 4 and the improved rate constant is in excellent agreement with the experimental value. More remarkable, the rate constant of the second reaction, involving acetone oxide [$(CH_3)_2COO$], is increased by a factor of 10. Our final rate constant, $(2.8\pm1.3)\times10^{-15}$ cm^3 s^{-1}, is just one order of magnitude less than the experimental value of $(4.29\pm0.54)\times10^{-14}$ cm^3 s^{-1}. This substantial improvement is expected, as larger systems will have greater deviations from the RRHO partition function approximation due to an increased number of torsional modes and anharmonicity. We believe that the remaining discrepancy could be diminished by the inclusion of anharmonic corrections for the partition functions and ZPVEs. To

Table 3 Reaction rate constants computed using Canonical Transition State Theory (CTST) and available experimental data. In this work, uncertainties are taken as the interval between CCSD(T)/CBS+Δ and the CCSD(T)/CBS+Δ+$\Delta_{T(Q)}$ computed rates, whereas central values are the average of them, as shown in equation 10

Ref.	Method	Temperature (K)	k_{tot} ($cm^3\ s^{-1}$)
$CH_3OH + H_2COO \longrightarrow CH_3OCH_2OOH$			
25	RRHO[a]	298.15	2.5×10^{-13}
69	RRHO[b]	298.15	1.2×10^{-14}
This work	RRHO	298.15	$(3.0\pm1.8)\times10^{-14}$
This work	1-D HR	298.15	$(1.2\pm0.8)\times10^{-13}$
25	Exp.	295	$(1.4\pm0.4)\times10^{-13}$
24	Exp.	292.6	$(1.04\pm0.02)\times10^{-13}$
$CH_3OH + (CH_3)_2COO \longrightarrow CH_3OC(CH_3)_2OOH$			
69	RRHO[a]	298.15	5.68×10^{-16}
This work	RRHO	298.15	$(2.8\pm1.3)\times10^{-16}$
This work	1-D HR	298.15	$(2.8\pm1.3)\times10^{-15}$
24	Exp.	292.6	$(4.29\pm0.54)\times10^{-14}$

[a] CCSD(T)/aug-cc-pVTZ//CCSD/cc-pVDZ

[b] DF-CCSD(T)-F12a/aug-cc-pVTZ//B3LYP/cc-pVTZ

model the kinetics of these system, we need not only accurate energies, but also accurate partition functions. The RRHO approximation underestimates the partition function values, which lead to a smaller rate constant. On the other hand, lower levels of theory tends to underestimate the transition state barrier, which leads to a larger rate constant. Therefore, it can be understood how cancellation of errors could give the right answer for the wrong reason.

3.3.3 Temperature dependence.

We computed the total rate constant for both systems over a range of temperatures using all combinations of methods employed herein; the results are presented in Figures 5 and 6. We found that the key factor that commands the temperature dependence is the energy component in equation 8, that is, the relative energy of the transition state. For the formaldehyde oxide system, the energy of the transition state is negative (i.e., below the reagents). Thus, the factor $e^{-\frac{E_{TS}}{k_B T}}$ gives the overall rate constant a negative temperature dependence. In contrast, for the acetone oxide reaction the energy of the transition state is positive, rising above the reagents, thus the factor $e^{-\frac{E_{TS}}{k_B T}}$ contributes positively. We can conclude that the reason formaldehyde oxide (H_2COO) and acetone oxide [$(CH_3)_2COO$] display, respectively, direct and inverse temperature dependence at high temperature is mainly due the barrier height of the reaction. When methanol reacts with formaldehyde oxide (H_2COO), it encounters a submerged barrier, whereas for acetone oxide [$(CH_3)_2COO$] it has to overcome a positive barrier. This does not yet explain the negative temperature dependence observed for the acetone oxide system at low temperatures. Watson and coworkers[69] suggested that the presence of mixed temperature dependence for that system could be caused by additional reaction channels. We show, however, that such mixed behaviour is obtained by considering only one reaction channel. Moreover, we demonstrate here in Figure 6 that this mixed temperature behaviour can only be achieved, within this model, if a tunneling factor is included. As temperature decreases the classical reaction rate (without tunneling contribution) gets smaller, but the transmission coefficient (κ) increases. Hence, the combination of both factors gives rise to a parabola-shaped curve. This indicates that the complex behaviour of the acetone oxide system might be explained by a combination of the energetically-driven positive temperature dependence and the tunneling-driven negative temperature dependence. Similar behaviour cannot be observed for the simpler SCI because there both the energetic and the tunneling factors contribute negatively as temperature is increased. It is important to notice, however, that we only get a minimum point close to the experimentally observed turning point (which is around 290 K)[24] under the rigid rotor approximation.

The inclusion of free and hindered rotors enhances the positive contribution for the temperature dependence, overcoming the negative contribution of the transmission coefficient. This indicates that further corrections in this model would still impact the predicted qualitative behaviour. The inclusion of more pathways, as proposed by Watson and coworkers, could improve kinetic rate constant, but only in the high temperature region, thus it could not account for the lack a negative temperature dependence observed in the 1D HR approach. Since overall the CCSD(T)/CBS+Δ energies are in better agreement with experimental data, we suspect that the real transition state barrier could be slight lower than predicted with our combined method. If this barrier is submerged with respect to the reagents, there will be no positive contribution from the energy factor. We discuss in our Supporting Information that in this case the mixed temperature dependence would arise from an entropy factor.

4 Conclusions

We have used high-level *ab initio* methods to study the addition of methanol to formaldehyde oxide (H_2COO) and acetone oxide [$(CH_3)_2COO$]. Geometries obtained at the CCSD(T)/ANO1 level of theory indicate that the zwitterionic character of the SCI changes depending on the substituent. The π character of the C−O bonds increases as methyl groups are added to the Criegee intermediate. We obtain a large contribution to correlation energy due to high-order dynamic correlation ($\Delta_{T(Q)}$). The full inclusion of such a correction, however, seems to move our kinetic results away from the experimental values. A computation of heat of formation for the simplest Criegee also shows that the $\Delta_{T(Q)}$ displaces our value from the reference value. Following these results, we conclude that the perturbative quadruples treatment for this system, combined with an insufficient sized basis set, might overestimate the contribution of full quadruple excitations. Future work could address the energy convergence for Criegee intermediates at high-order coupled cluster theory.

Energy profiles for the reactions R1 and R2 are reported, where the $\Delta_{T(Q)}$ contribution was employed to estimate our range of uncertainty. In both reactions, we observed a formation of a prereactive complex followed by a transition state that leads to the alkoxyalkyl hydroperoxide product. The key difference between the two reactions studied was the height of the transition state

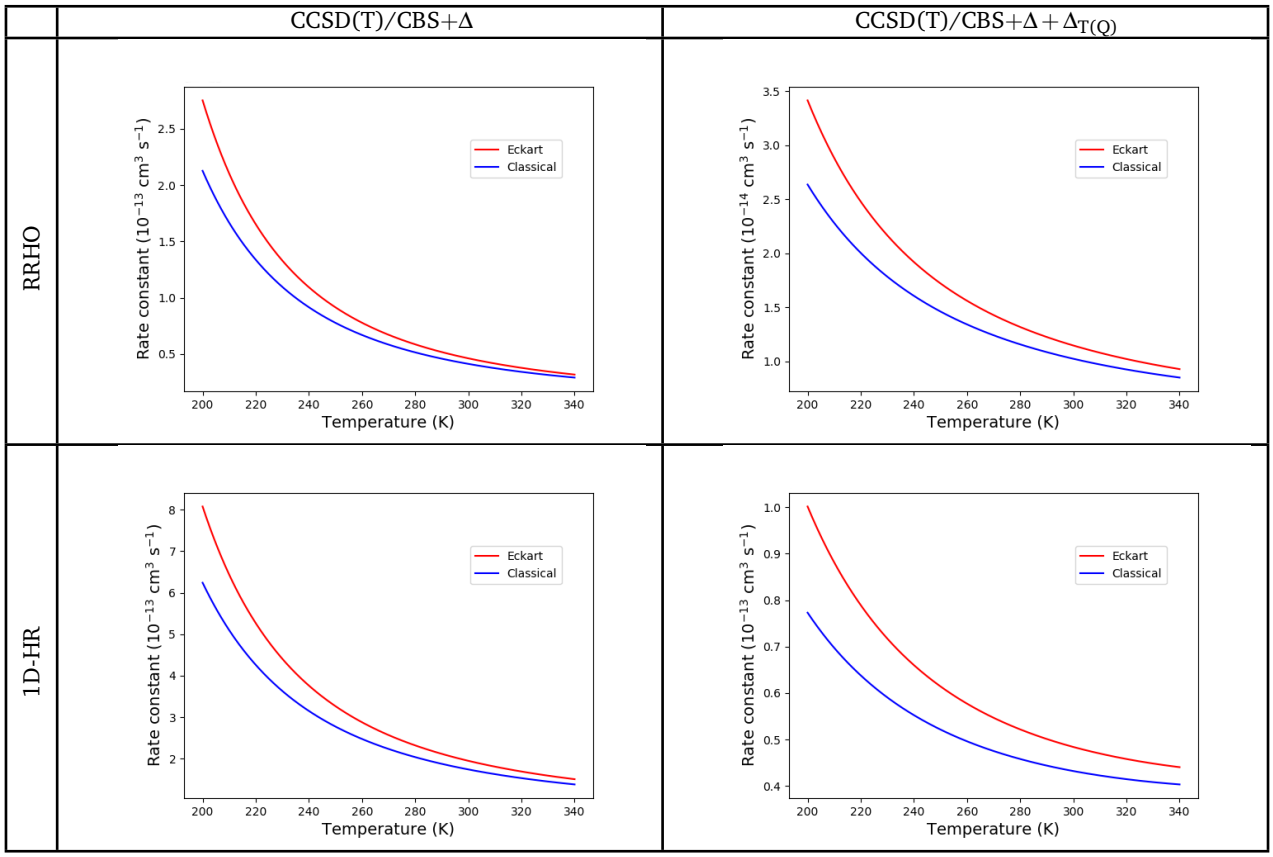

Fig. 5 Kinetic rate constant as a function of temperature without tunneling contribution (blue line) and with an Eckart transmission coefficient (red line) for the reaction R1 of methanol and formaldehyde oxide (H_2COO) under different combinations of methods.

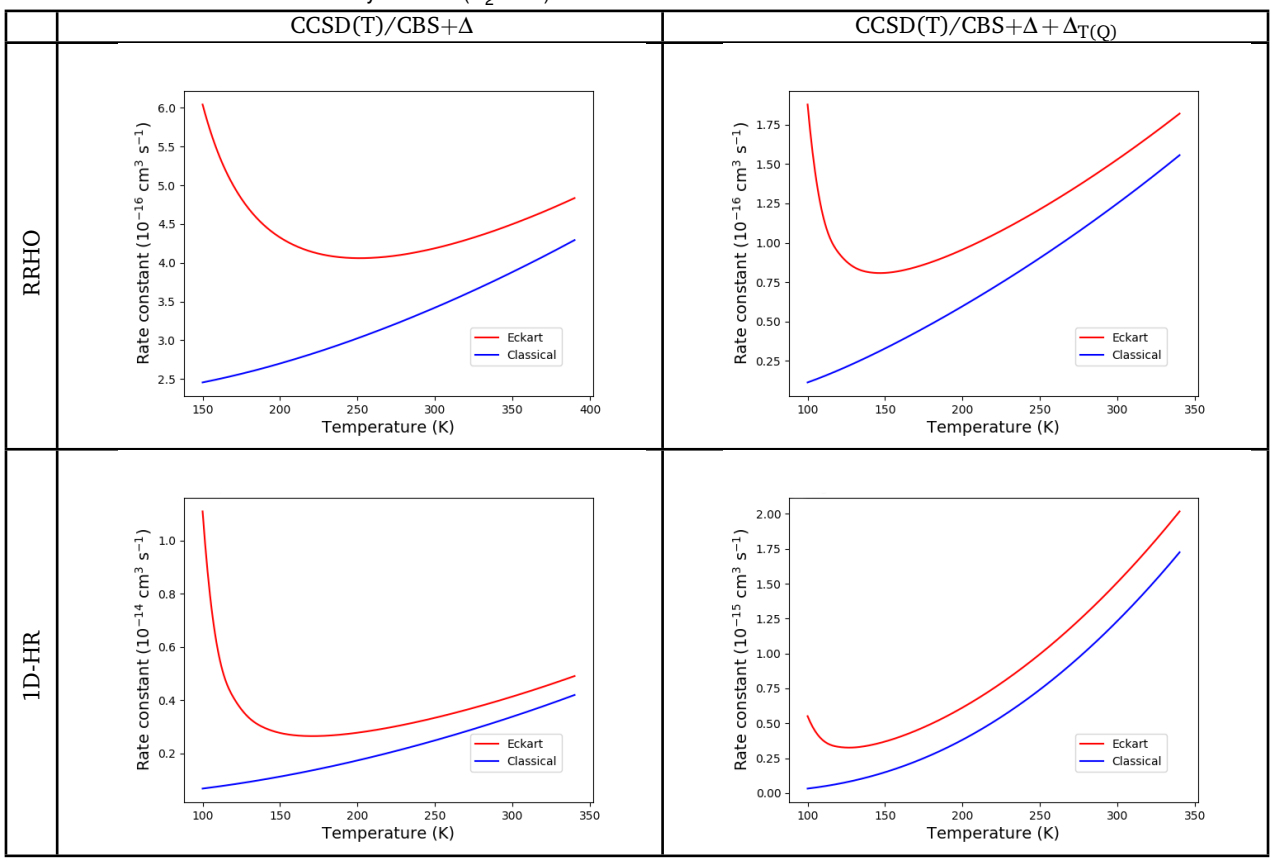

Fig. 6 Kinetic rate constant as a function of temperature without tunneling contribution (blue line) and with an Eckart transmission coefficient (red line) for the reaction R2 of methanol and acetone oxide [$(CH_3)_2COO$] under different combinations of methods.

barriers: for the simplest SCI this barrier is submerged, whereas for the methylated analogue the barrier rises above the reagents. This can be understood by examining the steric hindrance created by the methyl substituents around the carbonyl group and reflects on the lower kinetic rate computed. The CTST along with the RRHO approximation was used to compute kinetic rates. The computed rate constant for reaction R1 under the RRHO approximation is $(3.0\pm1.8)\times10^{-14}$ cm^3 s^{-1}, which is only about a factor of 3 smaller than the experimental value. However, the same approach leads to a rate constant two orders of magnitude smaller than expected for reaction R2. The inclusion of a 1-D hindered rotor treatment of low energy vibrational modes corresponding to torsions was employed to refine the partition functions. This approach was found to be particularly important for the acetone oxide system, where the rate of reaction improved by a factor of 10. The final rate constants for reactions R1 and R2 are $(1.2\pm0.8)\times10^{-13}$ and $(2.8\pm1.3)\times10^{-15}$ cm^3 s^{-1}, respectively. The former is in excellent agreement with experiment, whereas the latter is within an order of magnitude.

The experimental observation[24] of a dual temperature dependence for the rate constant of the reaction of methanol and acetone oxide was also investigated. We found that the height of the transition state barrier commands this behavior, as also noted by Watson and coworkers.[69] However, our results challenge the suggestion that multiple reaction paths cause the mixed temperature dependence. We show that with only the lowest energy path being considered, the positive and negative regions are obtained when tunneling contributions are included onto the RRHO approach. Hence, within this model, tunneling contributes to the qualitative description of the system. The lower bound energy for this reaction transition state barrier is slightly positive (0.24 kcal mol^{-1}); however, treatments beyond what was applied here, such as anharmonic treatment of the ZPVE, could move this barrier. If such treatments bring the barrier below the reagents, the qualitative interpretation will change. Since the inclusion of 1-D hindered rotors displace the minimum $k_{\mathrm{tot}}(T)$ from the experimentally observed temperature, we conclude that there is still room for improvement, though it is unclear whether better treatments than those presented herein would be tractable. Nevertheless, more elaborate methods for kinetics rates or tunneling contributions may be employed in the future to further study and model this challenging system.

Conflicts of interest

There are no conflicts to declare.

Acknowledgements

This research was supported by the U.S. Department of Energy (DOE), Office of Science, Office of Basic Energy Sciences (BES) under Contract No. DE-SC0018412.

References

1 R. Criegee, *Angew. Chem. Int. Ed.*, 1975, **14**, 745–752.
2 C. A. Taatjes, G. Meloni, T. M. Selby, A. J. Trevitt, D. L. Osborn, C. J. Percival and D. E. Shallcross, *J. Am. Chem. Soc.*, 2008, **130**, 11883–11885.
3 O. Welz, J. D. Savee, D. L. Osborn, S. S. Vasu, C. J. Percival, D. E. Shallcross and C. A. Taatjes, *Science*, 2012, **335**, 204–207.
4 P. S. Monks, A. T. Archibald, A. Colette, O. Cooper, M. Coyle, R. Derwent, D. Fowler, C. Granier, K. S. Law, G. E. Mills, D. S. Stevenson, O. Tarasova, V. Thouret, E. Von Schneidemesser, R. Sommariva, O. Wild and M. L. Williams, *Atmos. Chem. Phys.*, 2015, **15**, 8889–8973.
5 T. L. Nguyen, H. Lee, D. A. Matthews, M. C. McCarthy and J. F. Stanton, *J. Phys. Chem. A*, 2015, **119**, 5524–5533.
6 M. Campos-Pineda and J. Zhang, *Chem. Phys. Lett.*, 2017, **683**, 647–652.
7 D. Johnson and G. Marston, *Chem. Soc. Rev.*, 2008, **37**, 699.
8 R. L. Mauldin, T. Berndt, M. Sipilä, P. Paasonen, T. Petäjä, S. Kim, T. Kurtén, F. Stratmann, V. M. Kerminen and M. Kulmala, *Nature*, 2012, **488**, 193–196.
9 A. B. Ryzhkov and P. A. Ariya, *Phys. Chem. Chem. Phys.*, 2004, **6**, 5042–5050.
10 J. M. Anglada, J. González and M. Torrent-Sucarrat, *Phys. Chem. Chem. Phys.*, 2011, **13**, 13034–13045.
11 K. E. Leather, M. R. McGillen, M. C. Cooke, S. R. Utembe, A. T. Archibald, M. E. Jenkin, R. G. Derwent, D. E. Shallcross and C. J. Percival, *Atmos. Chem. Phys.*, 2012, **12**, 469–479.
12 M. C. Smith, C. H. Chang, W. Chao, L. C. Lin, K. Takahashi, K. A. Boering and J. J. M. Lin, *J. Phys. Chem. Lett.*, 2015, **6**, 2708–2713.
13 W. Chao, J. T. Hsieh, C. H. Chang and J. J. M. Lin, *Science*, 2015, **347**, 751–754.
14 C. A. Taatjes, O. Welz, A. J. Eskola, J. D. Savee, A. M. Scheer, D. E. Shallcross, B. Rotavera, E. P. F. Lee, J. M. Dyke, D. K. W. Mok, D. L. Osborn and C. J. Percival, *Science*, 2013, **340**, 177–180.
15 G. Sarwar, H. Simon, K. Fahey, R. Mathur, W. S. Goliff and W. R. Stockwell, *Atmos. Environ.*, 2014, **85**, 204–214.
16 T. Berndt, T. Jokinen, M. Sipilä, R. L. Mauldin, H. Herrmann, F. Stratmann, H. Junninen and M. Kulmala, *Atmos. Environ.*, 2014, **89**, 603–612.
17 R. Chhantyal-Pun, A. Davey, D. E. Shallcross, C. J. Percival and A. J. Orr-Ewing, *Phys. Chem. Chem. Phys.*, 2015, **17**, 3617–3626.
18 J. P. Misiewicz, S. N. Elliott, K. B. Moore and H. F. Schaefer, *Phys. Chem. Chem. Phys.*, 2018, **20**, 7479–7491.
19 S. Jørgensen and A. Gross, *J. Phys. Chem. A*, 2009, **113**, 10284–10290.
20 O. Welz, A. J. Eskola, L. Sheps, B. Rotavera, J. D. Savee, A. M. Scheer, D. L. Osborn, D. Lowe, A. Murray Booth, P. Xiao, M. A. H. Khan, C. J. Percival, D. E. Shallcross and C. A. Taatjes, *Angew. Chem. Int. Ed.*, 2014, **53**, 4547–4550.
21 R. Chhantyal-Pun, M. R. McGillen, J. M. Beames, M. A. H. Khan, C. J. Percival, D. E. Shallcross and A. J. Orr-Ewing, *Angew. Chem. Int. Ed.*, 2017, **56**, 9044–9047.
22 W. M. Wei, X. Yang, R. H. Zheng, Y. D. Qin, Y. K. Wu and F. Yang, *Comput. Theor. Chem.*, 2015, **1074**, 142–149.

23 R. M. Elsamra, A. Jalan, Z. J. Buras, J. E. Middaugh and W. H. Green, *Int. J. Chem. Kinet.*, 2016, **48**, 474–488.

24 M. R. McGillen, B. F. Curchod, R. Chhantyal-Pun, J. M. Beames, N. Watson, M. A. H. Khan, L. McMahon, D. E. Shallcross and A. J. Orr-Ewing, *ACS Earth Sp. Chem.*, 2017, **1**, 664–672.

25 S. V. Tadayon, E. S. Foreman and C. Murray, *J. Phys. Chem. A*, 2018, **122**, 258–268.

26 S. Enami and A. J. Colussi, *J. Phys. Chem. A*, 2017, **121**, 5175–5182.

27 Y. Sakamoto, R. Yajima, S. Inomata and J. Hirokawa, *Phys. Chem. Chem. Phys.*, 2017, **19**, 3165–3175.

28 R. Chhantyal-Pun, O. Welz, J. D. Savee, A. J. Eskola, E. P. Lee, L. Blacker, H. R. Hill, M. Ashcroft, M. A. H. Khan, G. C. Lloyd-Jones, L. Evans, B. Rotavera, H. Huang, D. L. Osborn, D. K. Mok, J. M. Dyke, D. E. Shallcross, C. J. Percival, A. J. Orr-Ewing and C. A. Taatjes, *J. Phys. Chem. A*, 2017, **121**, 4–15.

29 H.-L. Huang, W. Chao and J. J.-M. Lin, *Proc. Natl. Acad. Sci.*, 2015, **112**, 10857–10862.

30 L. Vereecken, A. Novelli and D. Taraborrelli, *Phys. Chem. Chem. Phys.*, 2017, **19**, 31599–31612.

31 T. B. Nguyen, G. S. Tyndall, J. D. Crounse, A. P. Teng, K. H. Bates, R. H. Schwantes, M. M. Coggon, L. Zhang, P. Feiner, D. O. Milller, K. M. Skog, J. C. Rivera-Rios, M. Dorris, K. F. Olson, A. Koss, R. J. Wild, S. S. Brown, A. H. Goldstein, J. A. de Gouw, W. H. Brune, F. N. Keutsch, J. H. Seinfeld and P. O. Wennberg, *Phys. Chem. Chem. Phys.*, 2016, **18**, 10241–10254.

32 P. Neeb, O. Horie and G. K. Moortgat, *Int. J. Chem. Kinet.*, 1996, **28**, 721–730.

33 M. Yang, P. D. Nightingale, R. Beale, P. S. Liss, B. Blomquist and C. Fairall, *Proc. Natl. Acad. Sci.*, 2013, **110**, 20034–20039.

34 T. Stavrakou, A. Guenther, A. Razavi, L. Clarisse, C. Clerbaux, P. F. Coheur, D. Hurtmans, F. Karagulian, M. De Mazière, C. Vigouroux, C. Amelynck, N. Schoon, Q. Laffineur, B. Heinesch, M. Aubinet, C. Rinsland and J. F. Müller, *Atmos. Chem. Phys.*, 2011, **11**, 4873–4898.

35 J. H. Kroll and J. H. Seinfeld, *Atmos. Environ.*, 2008, **42**, 3593–3624.

36 M. A. Khan, C. J. Percival, R. L. Caravan, C. A. Taatjes and D. E. Shallcross, *Environ. Sci. Process. Impacts*, 2018, **20**, 437–453.

37 H. J. Tobias and P. J. Ziemann, *J. Phys. Chem. A*, 2001, **105**, 6129–6135.

38 M. Nakajima and Y. Endo, *J. Chem. Phys.*, 2013, **139**, 101103.

39 Y. Fang, F. Liu, S. J. Klippenstein and M. I. Lester, *J. Chem. Phys.*, 2016, **145**, 044312–044320.

40 B. Long, J. L. Bao and D. G. Truhlar, *J. Am. Chem. Soc.*, 2016, **138**, 14409–14422.

41 J. Almlöf and P. R. Taylor, *J. Chem. Phys.*, 1987, **86**, 4070–4077.

42 J. Almlöf and P. R. Taylor, *J. Chem. Phys.*, 1990, **92**, 551–560.

43 A. L. L. East and W. D. Allen, *J. Chem. Phys.*, 1993, **99**, 4638–4650.

44 A. G. Császár, W. D. Allen and H. F. Schaefer, *J. Chem. Phys.*, 1998, **108**, 1007–11599.

45 M. S. Schuurman, S. R. Muir, W. D. Allen and H. F. Schaefer, *J. Chem. Phys.*, 2004, **120**, 11586–11599.

46 T. H. Dunning, *J. Chem. Phys.*, 1989, **90**, 1007–1023.

47 D. Feller, *J. Chem. Phys.*, 1992, **96**, 6104–6114.

48 D. Feller, *J. Chem. Phys.*, 1993, **98**, 7059–7071.

49 T. Helgaker, W. Klopper, H. Koch and J. Noga, *J. Chem. Phys.*, 1997, **106**, 9639–9646.

50 K. A. Peterson and T. H. Dunning, *J. Chem. Phys.*, 2002, **117**, 10548–10560.

51 H. Sellers and P. Pulay, *Chem. Phys. Lett.*, 1984, **103**, 463–465.

52 N. C. Handy, Y. Yamaguchi and H. F. Schaefer III, *J. Chem. Phys.*, 1986, **84**, 4481–4484.

53 K. G. Dyall, *J. Chem. Phys.*, 1997, **106**, 9618–9626.

54 W. Kutzelnigg and W. Liu, *J. Chem. Phys.*, 2005, **123**, 241102.

55 W. Liu and D. Peng, *J. Chem. Phys.*, 2006, **125**, 044102.

56 M. Iliaš and T. Saue, *J. Chem. Phys.*, 2007, **126**, 064102.

57 J. Sikkema, L. Visscher, T. Saue and M. Iliaš, *J. Chem. Phys.*, 2009, **131**, 124116.

58 W. Liu and D. Peng, *J. Chem. Phys.*, 2009, **131**, 031104.

59 H.-J. Werner, P. J. Knowles, G. Knizia, F. R. Manby, M. Schütz, P. Celani, T. Korona, R. Lindh, A. Mitrushenkov, G. Rauhut, K. R. Shamasundar, T. B. Adler, R. D. Amos, A. Bernhardsson, A. Berning, D. L. Cooper, M. J. O. Deegan, A. J. Dobbyn, F. Eckert, E. Goll, C. Hampel, A. Hesselmann, G. Hetzer, T. Hrenar, G. Jansen, C. Köppl, Y. Liu, A. W. Lloyd, R. A. Mata, A. J. May, S. J. McNicholas, W. Meyer, M. E. Mura, A. Nicklass, D. P. O'Neill, P. Palmieri, K. Pflüger, R. Pitzer, M. Reiher, T. Shiozaki, H. Stoll, A. J. Stone, R. Tarroni, T. Thorsteinsson, M. Wang and A. Wolf, *MOLPRO, version 2010.1, a Package of Ab Initio Programs*, 2010, see http://www.molpro.net.

60 CFOUR, a quantum chemical program package written by J.F. Stanton, J. Gauss, L. Cheng, M.E. Harding, D.A. Matthews, and P.G. Szalay with contributions from A.A. Auer, R.J. Bartlett, U. Benedikt, C. Berger, D.E. Bernholdt, Y.J. Bomble, O. Christiansen, F. Engel, R. Faber, M. Heckert, O. Heun, C. Huber, T.-C. Jagau, D. Jonsson, J. Jusélius, K. Klein, W.J. Lauderdale, F. Lipparini, T. Metzroth, L.A. Mück, D.P. OâĂŹNeill, D.R. Price, E. Prochnow, C. Puzzarini, K. Ruud, F. Schiffmann, W. Schwalbach, C. Simmons, S. Stopkowicz, A. Tajti, J. Vázquez, F. Wang, J.D. Watts and the integral packages MOLECULE (J. Almlöf and P.R. Taylor), PROPS (P.R. Taylor), ABACUS (T. Helgaker, H.J. Aa. Jensen, P. Jørgensen, and J. Olsen), and ECP routines by A. V. Mitin and C. van Wüllen. For the current version, see http://www.cfour.de.

61 R. M. Parrish, L. A. Burns, D. G. Smith, A. C. Simmonett, A. E. DePrince, E. G. Hohenstein, U. Bozkaya, A. Y. Sokolov, R. Di Remigio, R. M. Richard, J. F. Gonthier, A. M. James, H. R. McAlexander, A. Kumar, M. Saitow, X. Wang, B. P. Pritchard, P. Verma, H. F. Schaefer, K. Patkowski, R. A. King, E. F. Valeev, F. A. Evangelista, J. M. Turney, T. D. Crawford and C. D. Sherrill, *J. Chem. Theory Comput.*, 2017, **13**, 3185–3197.

62 Y. Georgievskii, J. A. Miller, M. P. Burke and S. J. Klippenstein,

J. Phys. Chem. A, 2013, **117**, 12146–12154.
63 Y. Georgievskii and S. J. Klippenstein, MESS.2016.3.23.
64 W. H. Bunnelle, *Chem. Rev.*, 1991, **91**, 335–362.
65 D. Cremer, J. Gauss, E. Kraka, J. F. Stanton and R. J. Bartlett, *Chem. Phys. Lett.*, 1993, **209**, 547–556.
66 M. T. Nguyen, T. L. Nguyen, V. T. Ngan and H. M. T. Nguyen, *Chem. Phys. Lett.*, 2007, **448**, 183–188.
67 Y. T. Su, Y.-H. Huang, H. A. Witek and Y.-P. Lee, *Science*, 2013, **340**, 174–176.
68 Y. T. Su, H. Y. Lin, R. Putikam, H. Matsui, M. C. Lin and Y. P. Lee, *Nat. Chem.*, 2014, **6**, 477–483.
69 N. A. I. Watson, J. A. Black, T. M. Stonelake, P. J. Knowles and J. M. Beames, *J. Phys. Chem. A*, 2018, **123**, 218–229.
70 T. J. Lee and P. R. Taylor, *Int. J. Quantum Chem.*, 2009, **36**, 199–207.
71 B. Ruscic, R. E. Pinzon, M. L. Morton, G. von Laszevski, S. J. Bittner, S. G. Nijsure, K. A. Amin, M. Minkoff and A. F. Wagner, *J. Phys. Chem. A*, 2004, **108**, 9979–9997.
72 B. Ruscic, R. E. Pinzon, G. von Laszewski, D. Kodeboyina, A. Burcat, D. Leahy, D. Montoy and A. F. Wagner, *J. Phys. Conf. Ser.*, 2005, **16**, 561–570.
73 B. Ruscic and D. H. Bross, *Active Thermochemical Tables (ATcT) values based on ver. 1.122d of the Thermochemical Network (2018)*, `https://atct.anl.gov/`.
74 K. J. Laidler, *Pure Appl. Chem.*, 1996, **68**, 149–192.
75 K. J. Laidler and M. C. King, *J. Phys. Chem.*, 1983, **87**, 2657–2664.
76 D. G. Truhlar, B. C. Garrett and S. J. Klippenstein, *J. Phys. Chem.*, 1996, **100**, 12771–12800.
77 Y. Liu, C. Yin, M. C. Smith, S. Liu, M. Chen, X. Zhou, C. Xiao, D. Dai, J. J.-M. Lin, K. Takahashi, W. Dong and X. Yang, *Phys. Chem. Chem. Phys.*, 2018, **20**, 29669–29676.
78 H. S. Johnston and J. Heicklen, *J. Phys. Chem.*, 1962, **66**, 532–533.
79 J. Espinosa-García, F. O. del Valle and J. Corchado, *Chemical Physics*, 1994, **183**, 95–100.

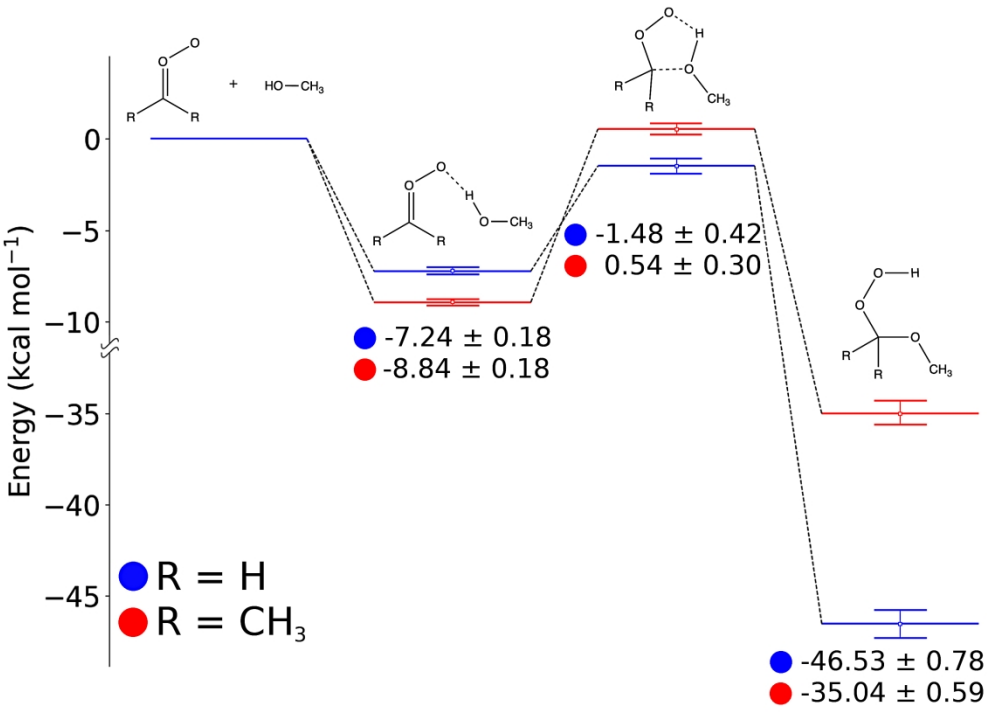
Energy (kcal mol^{-1})
0
−5
−10
−35
−40
−45
+ HO—CH$_3$
-7.24 ± 0.18
-8.84 ± 0.18
-1.48 ± 0.42
0.54 ± 0.30
-46.53 ± 0.78
-35.04 ± 0.59
R = H
R = CH$_3$